Available online at www.sciencedirect.com
ScienceDirect
Icarus 193 (2008) 387–396
ICARUS
www.elsevier.com/locate/icarus

Thermal convection in ice-I shells of Titan and Enceladus

Giuseppe Mitri [a,*], Adam P. Showman [b]

[a] Jet Propulsion Laboratory, California Institute of Technology, 4800 Oak Grove Drive, Pasadena, CA 91109, USA
[b] Department of Planetary Sciences and Lunar and Planetary Laboratory, University of Arizona, 1629 E. University Blvd., Tucson, AZ 85721, USA

Received 27 November 2006; revised 26 June 2007

Available online 6 September 2007

Abstract

Cassini–Huygens observations have shown that Titan and Enceladus are geologically active icy satellites. Mitri and Showman [Mitri, G., Showman, A.P., 2005. Icarus 177, 447–460] and McKinnon [McKinnon, W.B., 2006. Icarus 183, 435–450] investigated the dynamics of an ice shell overlying a pure liquid-water ocean and showed that transitions from a conductive state to a convective state have major implications for the surface tectonics. We extend this analysis to the case of ice shells overlying ammonia-water oceans. We explore the thermal state of Titan and Enceladus ice-I shells, and also we investigate the consequences of the ice-I shell conductive–convective switch for the geology. We show that thermal convection can occur, under a range of conditions, in the ice-I shells of Titan and Enceladus. Because the Rayleigh number *Ra* scales with δ^3/η_b, where δ is the thickness of the ice shell and η_b is the viscosity at the base of the ice-I shell, and because ammonia in the liquid layer (if any) strongly depresses the melting temperature of the water ice, *Ra* equals its critical value for two ice-I shell thicknesses: for relatively thin ice shell with warm, low-viscosity base (Onset I) and for thick ice shell with cold, high-viscosity base (Onset II). At Onset I, for a range of heat fluxes, two equilibrium states—corresponding to a thin, conductive shell and a thick, convective shell—exist for a given heat flux. Switches between these states can cause large, rapid changes in the ice-shell thickness. For Enceladus, we demonstrate that an Onset I transition can produce tectonic stress of ∼500 bars and fractures of several tens of km depth. At Onset II, in contrast, we demonstrate that *zero* equilibrium states exist for a range of heat fluxes. For a mean heat flux within this range, the satellite experiences oscillations in surface heat flux and satellite volume with periods of ∼50–800 Myr even when the interior heat production is constant or monotonically declining in time; these oscillations in the thermal state of the ice-I shell would cause repeated episodes of extensional and compressional tectonism.

Keywords: Enceladus; Geophysics; Ices; Interiors; Saturn, satellites; Titan

1. Introduction

Cassini–Huygens observations have shown that Titan and Enceladus are geologically active icy satellites (Elachi et al., 2006; Porco et al., 2006; Spencer et al., 2006; Lopes et al., 2007). The domes, flow-like features (Elachi et al., 2006; Lopes et al., 2007) and mountains (Radebaugh et al., 2006) present on Titan are the surface manifestation of internal processes active in the outer ice-I shell. Titan (mean radius ∼2575 km) should be at least partially differentiated into a rocky interior and an outer water layer (e.g., Grasset et al., 2000; Tobie et al., 2006). Accretion and differentiation probably caused widespread melting (at least in the outer layers), which would release ammonia and other trapped volatiles into the liquid layer (Lunine et al., 1983; Mousis et al., 2002). Grasset and Sotin (1996) have shown that the presence of ammonia can impede the complete refreezing of Titan's liquid layer, promoting the existence of a subsurface ocean of ammonia-water liquid below the ice-I shell. Tobie et al. (2005a) estimated that the present heat flux on Titan is $\sim 0.007\ \mathrm{W\,m^{-2}}$.

The south pole of Enceladus (mean radius ∼252 km) is geologically active at the present time, with elevated surface temperatures, fractures, and jets of water and fine grained particles (Porco et al., 2006; Spencer et al., 2006). Porco et al. (2006) suggested that the jets are probably vents associated with reservoirs of liquid water residing below the surface. Enceladus exhibits a complex tectonic history, with both extensional and compressional geologic features and a variety of surface ages that suggest a multibillion-year tectonic history (Kargel

* Corresponding author.
E-mail address: giuseppe.mitri@jpl.nasa.gov (G. Mitri).

0019-1035/$ – see front matter
doi:10.1016/j.icarus.2007.07.016

and Pozio, 1996; Squyres et al., 1983). Squyres et al. (1983) suggested that refreezing of a liquid layer in the interior of Enceladus can produce a global radial expansion and fracturing of the ice-I shell. Using ice rheology as understood at the time, Squyres et al. also addressed the issue of whether thermal convection can occur in Enceladus' ice-I shell; more recent work by Barr and McKinnon (2007a, 2007b) shows that ice-shell convection can occur on Enceladus if the ice grain size is less than ∼1 mm. Enceladus appears to be hydrostatically relaxed and could be a differentiated body (Dermott and Thomas, 1994; Schubert et al., 2007), although debate exists (e.g., Porco et al., 2006). Nimmo and Pappalardo (2006) suggested that the highly tectonized terrains at the south pole resulted from diapiric upwelling and satellite reorientation; the latter process can produce tectonic stresses of $\sim 10^2$ bars. Interestingly, although ammonia has repeatedly been suggested as an agent that would promote cryovolcanism (Stevenson, 1982; Croft et al., 1988; Kargel, 1992), the Cassini Ion and Neutral Mass Spectrometer (INMS) did not detect ammonia and obtained an upper limit ammonia abundance of 0.5% in the escaping plume (Waite et al., 2006). However, the plume reservoir may reside relatively close to the surface, and the ammonia abundance in the deep interior could well be greater. Spencer et al. (2006) suggested that at the south pole the heat flux is $\sim 0.2\ \mathrm{W\,m^{-2}}$; the heat flux may be orders of magnitude lower in other regions of Enceladus.

Recent work has suggested that the geological activity, resurfacing, tectonism and outgassing of Titan could be related to the onset of thermal convection in the ice-I shell. The thermal-orbital evolution model of Tobie et al. (2005b) showed that Titan's ice-I shell could have transitioned only recently (within the past ∼1 Gyr) from a conductive state to a convective state. Tobie et al. (2006) have proposed that a late onset of convection in the ice-I shell could dissociate the methane clathrates trapped in the ice and could produce episodic events of methane outgassing from the interior of the satellite. Mitri and Showman (2005) have demonstrated that at the critical Rayleigh number Ra_{cr}, convection jumps immediately into a finite-amplitude state for a fluid with strongly temperature-dependent viscosity. Under appropriate conditions, modest variations in the heat flux from the interior can force an ice-I shell to switch between a conductive and a convective state. In our previous work, we have shown that for the ice-I shell of Europa, the conductive-convective transition produces radial expansion of a cooling ice-I shell. The rapidity of these switches implies that the stress build up, hence extensive fractures, could occur. Successively, McKinnon (2006) has discussed the tectonic implications of the conductive–convective transitions for the ice-I shell of Callisto. Moore (2006) confirmed the existence of two equilibrium states (conductive and convective) of an ice shell for a given heat flux from the interior.

We explore the hypothesis that in the presence of an internal ocean, a conductive–convective transition of the ice-I shell can produce geological activity and induce formation of numerous surface structures. This work extends our previous study (Mitri and Showman, 2005) to the regime of satellites with ammonia-water oceans. In a satellite with a pure liquid-water ocean, as assumed by Mitri and Showman (2005), changes in the thickness of the ice shell cause only mild changes in the temperature (and hence viscosity) at the base of the shell. When ammonia is present in the ocean, however, changes in the ice shell thickness cause severe changes in the temperature and viscosity at the base of the shell. This leads to qualitatively new effects that we document here.

To demonstrate the mechanisms, we apply the model to Titan and Enceladus, which differ in radius by over an order of magnitude and therefore represent large and small end-members in the class of geologically active icy satellites. Although we focus here on Enceladus and Titan, our work may also apply to other mid-size icy bodies in the outer Solar System such as Miranda, Ariel, Triton, and Pluto if those objects ever contained internal oceans (Hussmann et al., 2006).

2. Model

Goldsby and Kohlstedt (2001) proposed a composite equation to account the combined strain rate $\dot{\varepsilon}$ of several deformation mechanisms of water ice as

$$\dot{\varepsilon} = \dot{\varepsilon}_{\mathrm{diff}} + \left(\frac{1}{\dot{\varepsilon}_{\mathrm{basal}}} + \frac{1}{\dot{\varepsilon}_{\mathrm{gbs}}}\right)^{-1} + \dot{\varepsilon}_{\mathrm{disl}}, \tag{1}$$

where $\dot{\varepsilon}_{\mathrm{diff}}$, $\dot{\varepsilon}_{\mathrm{basal}}$, $\dot{\varepsilon}_{\mathrm{gbs}}$, and $\dot{\varepsilon}_{\mathrm{disl}}$ are the strain rate of diffusion flow, basal slip, grain boundary sliding (GBS), and dislocation creep, respectively. The strain rate for a single mechanism $\dot{\varepsilon}_j$ can described as

$$\dot{\varepsilon}_j = \frac{A\sigma^n}{d^p} e^{-Q/RT}, \tag{2}$$

where A is a constant, σ is the differential stress, d is the grain size, R is the gas constant, Q is the activation energy, T is temperature, and n and p are constants. The predominant creep mechanism of water ice for low tidal stress is GBS in combination with diffusion creep (Durham et al., 1997; McKinnon, 1999, 2006; Showman and Han, 2004; Goldsby and Kohlstedt, 2001). For Enceladus, Barr and McKinnon (2007a, 2007b) showed that convection can occur only if $d < 1$ mm, depending on the ammonia concentration; volume-diffusion creep dominates over GBS for grain sizes smaller than ∼0.9 mm. Barr and Pappalardo (2005) showed that, for conditions relevant to the icy Galilean satellites, volume diffusion dominates over GBS in well-developed convection for grain sizes smaller than ∼1 mm; this analysis also applies to Titan if the ice-shell is relatively pure water ice. We therefore assume that diffusion creep is the dominant the creep mechanism. The flow law for diffusion creep is given by

$$\dot{\varepsilon} = \frac{A'\sigma\Omega}{RTd^2} D_0 e^{-Q/(RT)}, \tag{3}$$

where A' is a constant, Ω is the molar volume, and D_0 is a coefficient. The ice viscosity can be written as

$$\eta = \frac{RTd^2}{3A'\Omega D_0} e^{Q/(RT)}. \tag{4}$$

We adopt $A' = 14$, $\Omega = 1.97 \times 10^{-5}\ \mathrm{m^3}$, $D_0 = 9.1 \times 10^{-4}\ \mathrm{m^2\,s^{-1}}$, and $Q = 59.4\ \mathrm{kJ\,mol^{-1}}$ (McKinnon, 2006). We consider that the ice grain size ranges between 0.1 mm and 1 mm (McKinnon, 2006; Barr and McKinnon, 2007a).

Because of the high viscosity contrast between the surface and the bottom of the ice-I shells on Titan and Enceladus, convection must occur in the stagnant-lid regime (McKinnon, 1999). Several scaling laws of stagnant lid regime have been proposed (Solomatov, 1995; Moresi and Solomatov, 1995; Dumoulin et al., 1999; Deschamps and Sotin, 2000). We adopt the Dumoulin et al. scaling law.

The Rayleigh number defined at the base of the ice shell is given by

$$Ra_b = \frac{\alpha\rho g \Delta T \delta^3}{\kappa \eta_b}, \tag{5}$$

where α is the thermal expansivity of the ice, ρ is ice density, g is gravity, ΔT is the temperature difference between the bottom and the surface of the ice-I shell, δ is the thickness of the ice shell, κ is the thermal diffusivity, and η_b is the viscosity at the bottom of the ice-I shell. The Rayleigh number defined at the convective layer interior is given by

$$Ra_i = \frac{\alpha\rho g \Delta T \delta^3}{\kappa \eta_i}, \tag{6}$$

where η_i is the viscosity within the interior of the convective sublayer. The ratio between these Rayleigh numbers is (Solomatov and Moresi, 1996, 1997; McKinnon, 2006)

$$Ra_b \sim e \times Ra_i. \tag{7}$$

The Nusselt number Nu depends on the Rayleigh number Ra. For low Rayleigh number the Nusselt number is given by (Dumoulin et al., 1999)

$$Nu = 1.99\theta^{-1} Ra_i^{1/5}. \tag{8}$$

For higher Rayleigh number the Nusselt number is given by (Dumoulin et al., 1999)

$$Nu = 0.52\theta^{-4/3} Ra_i^{1/3}. \tag{9}$$

We will call these the 1/5 and 1/3 convective regimes, respectively. The parameter θ is given by (Solomatov and Moresi, 2000)

$$\theta = 1.2\frac{Q\Delta T}{RT_i^2}, \tag{10}$$

where T_i is the temperature in the interior of the convective sublayer. The temperature difference between the base and the convective interior is $T_b - T_i \sim RT_i^2/Q$ (Solomatov and Moresi, 2000), where T_b and T_i are the temperatures at the base of the ice shell and within the interior of the convective sublayer, respectively.

The critical Rayleigh number defined at the bottom of the ice-I shell for Newtonian rheology (diffusion creep) is given by (Solomatov, 1995)

$$Ra_{b,\mathrm{cr}} = 20.9\theta^4. \tag{11}$$

We approximate the surface heat flux as (see discussion in McKinnon, 2006)

$$F = \frac{621}{\delta'} \ln\left(\frac{T_b}{T_s}\right)\left(1 - \frac{\delta'}{R_S}\right) Nu \ \mathrm{W\,m^{-1}}, \tag{12}$$

Table 1
Physical parameters

Parameter	Symbol	Value	Dimension
Radius of Titan	R_T	2575	km
Radius of Enceladus	R_E	252	km
Gravity of Titan	g_T	1.35	$\mathrm{m\,s^{-2}}$
Gravity of Enceladus	g_E	0.114	$\mathrm{m\,s^{-2}}$
Surface temperature of Titan	T_s	94	K
Surface temperature of Enceladus	T_s	70	K
Thermal expansivity	α	$1.58 \cdot 10^{-4}$	$\mathrm{K^{-1}}$
Ice density	ρ	920	$\mathrm{kg\,m^{-3}}$

where δ' is the effective thickness of the ice-I shell and R_S is the satellite radius. Equation (12) includes the temperature dependence of the thermal conductivity of ice and the spherical geometry of the problem.

The bottom temperature of the ice-I shell is given by the melting temperature for ammonia-water at the relevant oceanic ammonia composition. Depending on the composition, ammonia can strongly depress the melting temperature of water ice. Consider a satellite with an internal ocean. If the ice-I shell is thin, the ocean must be thick, so the ammonia concentration is low and the melting temperature is relatively close to that for pure water. As the ice shell thickens, the ocean thins, the oceanic ammonia becomes concentrated, and the melting temperature plummets. This means that the temperature at the base of the ice shell drops too. For a given change in the thickness of the ice-I shell, the resulting change in the oceanic ammonia concentration depends on whether a silicate mantle or high-pressure ices underlie the ocean. For Enceladus, pressures are too small for high-pressure ices to form, so assuming the satellite is differentiated, a silicate mantle should underlie any ocean that exists. To calculate the dependence of oceanic ammonia concentration (hence melting temperature) on the ice-I shell thickness in this case, we used the phase diagram and assumed that the volume loss (gain) of the ice-I shell equals the volume gain (loss) of the ocean during any melting or freezing events. In the Titan case, the existence of high-pressure ices underneath any internal ocean complicates the picture, because ocean volume changes result not only from volume changes of the ice-I shell but from simultaneous volume changes in the high-pressure-ice layer too. Including these effects, Grasset et al. (2000) calculated the dependence of melting temperature on the ice-I shell thickness for Titan assuming NH_3/H_2O ratios of 5 and 15%, and we adopt their relationships for Titan. For Enceladus we adopt the ammonia-phase diagram proposed by Leliwa-Kopystynski et al. (2002) that is in agreement with the Grasset et al. phase diagram in a pressure range 0–300 MPa.

The model does not include tidal internal heating in the ice. The physical parameters used in the model are listed in Table 1.

3. Results and discussion

Illustrations of the internal structures explored in our model for a differentiated Titan and Enceladus are shown in Figs. 1 and 2, respectively. We assume that each satellite is differentiated into an outer ice/water layer overlying a silicate core.

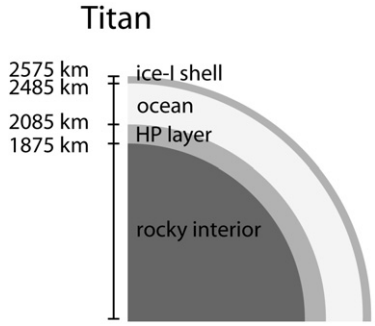

Fig. 1. Model of Titan's internal structure. Titan is differentiated into a rocky interior and an outer water layer of ∼700 km depth. The depth of the ice high pressure layer and the ice I shell is determined as in Grasset et al. (2000).

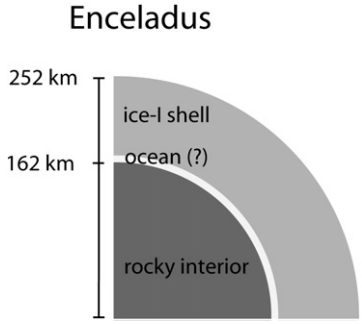

Fig. 2. Model of Enceladus' internal structure. We assume that Enceladus is differentiated into a rocky interior and an outer water layer.

We further assume that each body contains an internal liquid-water ocean. This assumption is reasonably plausible for Titan (Grasset et al., 2000; Tobie et al., 2005b), but less certain for Enceladus. Some authors have suggested a global internal liquid layer on Enceladus (Squyres et al., 1983), but other authors have proposed that any internal liquid regions are confined to localized reservoirs (Porco et al., 2006; Collins and Goodman, 2007).

For Titan mass $M_T = 1345.5 \times 10^{20}$ kg and Enceladus mass $M_E = 0.73 \times 10^{20}$ kg, and Titan radius $R_T = 2575$ km and Enceladus radius $R_E = 252$ km, we determine that the depth of the outer water layer of Titan is ∼700 km and the rocky interior radius is 1875 km, while the depth of Enceladus outer water layer is ∼90 km and the rocky interior radius is 162 km. However, for Titan, complete melting of the ice I shell leads to a state that still contains high-pressure ice (which lies between the ocean and the rock core) for realistic rock-core densities and radii. Under these conditions, the rock-core density and radius do not affect the functional dependence of oceanic ammonia concentration on the ice-I shell thickness. Therefore, our model does not require specification of Titan's rock-core density and radius. Our Titan models adopt a surface gravity of 1.35 m s^{-2}. For Enceladus $GM_E = 7.2085 \pm 0.0068$ km^3 s^{-2} (Porco et al., 2006), where G is the Newtonian gravitational constant. Therefore, we adopt for Enceladus a surface gravity of 0.114 m s^{-2}.

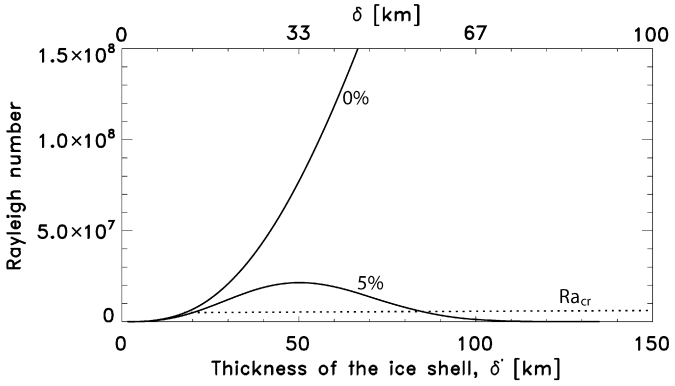

Fig. 3. Rayleigh number versus the thickness of the ice shell of Titan for initial ammonia-water fractions of 0 and 5% and ice grain size $d = 0.1$ mm (solid line). The dotted line shows the critical Rayleigh number.

3.1. Onset of thermal convection

Thermal convection in stagnant lid regime can occur in the ice shells of Titan and Enceladus. Fig. 3 shows the Rayleigh number dependence on the ice-shell thickness for Titan, for initial ammonia-water concentrations of 0 and 5%, and ice grain size 0.1 mm. For a pure water liquid layer the Rayleigh number increases with increasing thickness of the ice shell. For an ammonia-water ocean, because the Rayleigh number Ra scales as δ^3/η_b, where δ is the thickness of the ice shell and η_b is the viscosity at the base of the ice-I shell, and because the ammonia in the liquid layer strongly depresses the melting temperature of the ice, Ra is equal to its critical value for two critical thicknesses $\delta_{cr,I,II}$: for relatively thin ice shell ($\delta_{cr,I}$) with warm, low-viscosity base (Onset I) and for thick ice shell ($\delta_{cr,II}$) with cold, high-viscosity base (Onset II). For an initial ammonia concentration of 5%, the Rayleigh number Ra increases with increasing δ until reaching the maximum value at ∼50 km. For $\delta > 50$ km, the increasing η_b prevails over the δ^3 dependence, and the Rayleigh number decreases with increasing δ (Fig. 3; cf. the discussion in Sotin et al., 1997). Thus, depending on the ammonia concentration, conduction occurs for either thin or thick ice shells, while convection occurs for ice shells of intermediate thickness. In Fig. 3 we plot the Rayleigh number versus the effective thickness of the ice shell δ' (computed using Eq. (12)) that takes into account the temperature dependence of the ice thermal conductivity and Titan's spherical geometry. Fig. 3 shows also the thickness of the ice shell δ without considering the temperature dependence of the thermal conductivity and the spherical geometry of Titan. We note that $\delta' \sim 1.5\delta$.

For a fluid with temperature-dependent viscosity, at the critical Rayleigh number the Nusselt number is not a continuous function of the Rayleigh number, but has a finite amplitude discontinuity (Mitri and Showman, 2005; McKinnon, 2006). For the viscosity contrast expected in the satellite ice shells, at the critical Rayleigh number Ra_{cr} and in the convective regime the Nusselt number $Nu \sim 1.6$–1.7, while in the conductive regime $Nu = 1$. Consequently, with increasing ice-I shell thicknesses, we have two finite amplitude discontinuities of the Nusselt number: the first at $\delta_{cr,I}$ and the second at $\delta_{cr,II}$. This situation differs from the case of satellites with little ammonia (Mitri and

Showman, 2005), where the weak dependence of basal viscosity on ice-shell thickness implies that *Ra* is a monotonically increasing function of δ, and hence that only transition $\delta_{cr,I}$ exists.

3.2. Thermal state of Titan and Enceladus ice-I shells

Figs. 4 and 5, which follow the graphical representation used by McKinnon (2006), summarize the results on the thermal state of the ice-I shells on Titan and Enceladus, respectively. For assumed ice-shell rheology, material properties (density, thermal expansivity, thermal diffusivity), surface temperature, and gravity, the state of the ice shell (convective or conductive) and Nusselt number are functions of two main variables: the ice-shell thickness and the temperature (hence viscosity) at the base of the ice shell. Figs. 4 and 5 show contour plots of the heat flux as a function of these two parameters for conditions relevant to Titan and Enceladus. We present Titan models for three ice grain size (0.1, 0.5, and 1.0 mm). The Enceladus model assumes 0.1 mm grain size (Fig. 5). The basal temperature of the ice-I shell equals the subsurface ocean temperature (left vertical axes). The right vertical axes give the corresponding basal viscosity of the ice shell. The solid lines show the heat flux (tidal and radiogenic) from the interior of the satellite in $\mathrm{W\,m^{-2}}$. We plot in dashed–dotted lines the critical Rayleigh number: the heat flux is transported by thermal conduction in the overhanging part of the plot (gray area) and by thermal convection in the underlying (white area). The dotted lines show the Rayleigh number corresponding to the 1/5–1/3 convective transition: the 1/5 convective regime above the dotted line and 1/3 convective regime below the dotted line.

The dashed curves in Figs. 4 and 5 show the locus of basal temperatures/viscosities, heat fluxes, and ice-shell thicknesses for a specified initial ammonia-water concentration (0, 5, and 15% for Titan in Fig. 4, and 0, 0.5, 1.0, 1.5, 2.0, and 3.0% for Enceladus in Fig. 5). Therefore, each point along a dashed line represents a possible state of the ice shell for that initial ammonia-water concentration. For a given mass of total ammonia, the system must remain along the relevant dashed curve as the heat flux changes. The dashed curves therefore correspond to evolutionary trajectories: depending on the history of radiogenic and tidal heating, the system can slide up or down a dashed curve, but it cannot switch from one dashed curve to another. For example, assuming an initial ammonia mass concentration of 5%, grain size of 0.1 mm, and heat flux of $0.035\ \mathrm{W\,m^{-2}}$, Titan's ice shell is in the conductive state with a thickness of ∼18 km, while for a heat flux of $0.015\ \mathrm{W\,m^{-2}}$ the ice shell is in a convective state in 1/5 regime with a thickness of ∼70 km. A heat flux change from $0.035\ \mathrm{W\,m^{-2}}$ to $0.015\ \mathrm{W\,m^{-2}}$ produces an ice shell thickening of ∼52 km. During this decrease of heat flux, the ice-I shell switches from a conductive to a convective state, passing through Onset I.

To clarify these evolutionary trajectories, Fig. 6 shows the heat flux F versus ice-shell thickness δ for Titan for initial ammonia concentrations of 0, 5, and 15%, assuming that the grain size is 0.1 mm. In other words, we plot the $F(\delta)$ relationships defined by the three dashed curves in the top panel of Fig. 4.

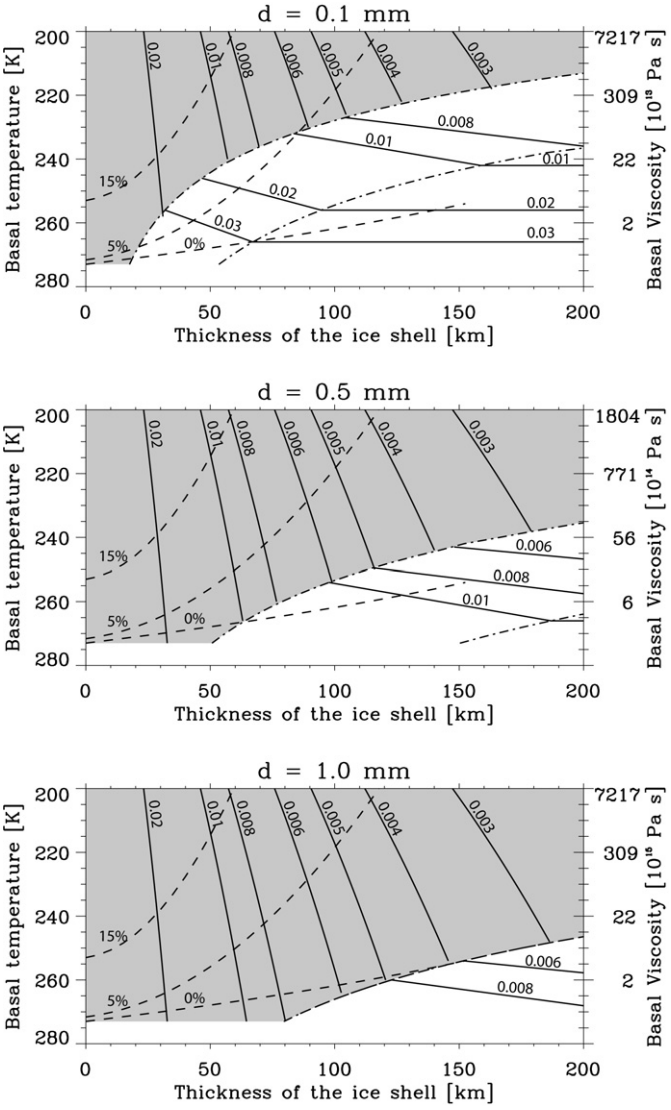

Fig. 4. Dependence of the heat flux of Titan's ice-I shell (conductive state, 1/5 convective regime and 1/3 convective regime) on the basal temperature and the thickness of the ice shell of Titan. The basal temperature of the ice shell corresponds to the ammonia-water ocean temperature (left vertical axis). The right vertical axis gives the viscosity of the bottom of the ice shell. The thermal state of the ice shell depends on the tidal and radiogenic heat flux (solid lines) from the interior of Titan and the primordial mass concentration of ammonia in the outer layer for 0, 5, 15% (dotted lines). The two plots consider three different ice grain size: 0.1, 0.5, and 1.0 mm. The dashed–dotted line shows the conductive–convective transition. The heat flux is transported by thermal conduction in the overhanging part of the plot (gray area) and by thermal convection in the underlying (white area). The dotted line shows the 1/5–1/3 transition regime of the thermal convection (1/5 in the overhanging part of the dotted line and 1/3 in the underlying); the solid lines show the heat flux (in $\mathrm{W\,m^{-2}}$) from the interior of the satellites (note that because of the jump in Nusselt number at critical Rayleigh number, the heat flux is not a continuous function of the thickness of ice shell, but instead encounters a discontinuity at the boundary between the white and gray regions).

The gray regions correspond to conductive shells and the white regions correspond to convective shells.

The first panel of Fig. 6 shows the dependence of heat flux on the ice-shell thickness for an initial ammonia-water concentration of 0% and $d = 0.1$ mm. For heat fluxes $F > 0.058\ \mathrm{W\,m^{-2}}$,

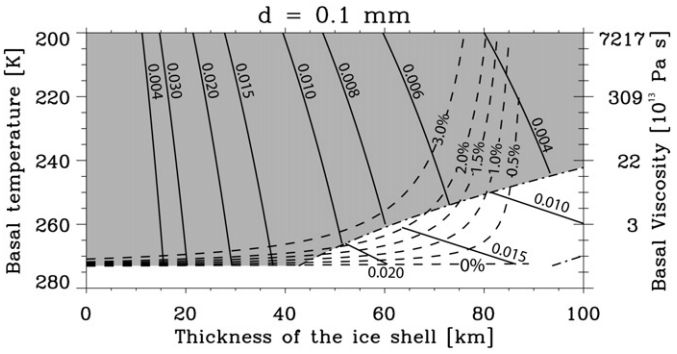

Fig. 5. Dependence of the thermal state of the Enceladus ice shell (conductive state, 1/5 convective regime and 1/3 convective regime) on the basal temperature and the thickness of the ice shell. The basal temperature of the ice shell corresponds to the ammonia-water ocean temperature (left-hand axis). The right-hand axis shows the viscosity of the bottom of the ice shell. The thermal state of the ice shell depends on the tidal and radiogenic heat flux (solid lines) from the interior of Titan and the primordial mass concentration of ammonia in the outer layer for 0, 0.5, 1.0, 1.5, 2.0, and 3.0% (dotted lines). The model considers an ice grain size of 0.1 mm. The dashed–dotted line shows the conductive–convective transition (the heat flux is transported for thermal conduction in the overhanging part of the plot and for thermal convection in the underlying); the dotted line shows the 1/5–1/3 transition regime of the thermal convection (1/5 above the dotted line and 1/3 below); the solid lines show the heat flux (in $\mathrm{W\,m^{-2}}$) from the interior of the satellites (note that because of the jump in Nusselt number at critical Rayleigh number, the heat flux is not a continuous function of the thickness of ice shell).

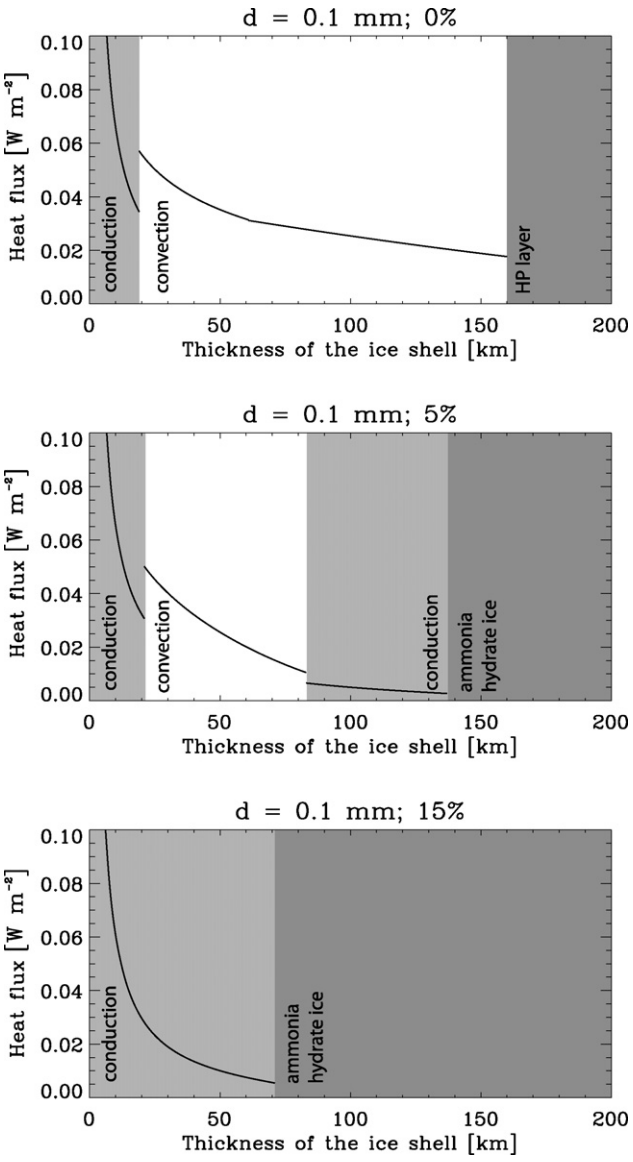

Fig. 6. Heat flux versus thickness of Titan's ice-I shell assuming heating from below. The model assumes an ice grain size $d = 1$ mm and three initial ammonia-water concentrations: 0, 5, and 15%. Grey and white areas show where the heat is transported though the ice-I shell by thermal conduction and convection, respectively. The graphite colored area show where the liquid layer crystallizes as high pressure ice and ammonia hydrate ice.

the shell must be thin and conductive, whereas for heat fluxes $F < 0.035\ \mathrm{W\,m^{-2}}$, the shell must be thick and convective. For heat fluxes between $0.035\ \mathrm{W\,m^{-2}}$ and $0.058\ \mathrm{W\,m^{-2}}$, two solutions exist for a given heat flux: one corresponding to a thin, conductive ice shell, and the other to a thick, convective ice shell (Mitri and Showman, 2005). At the critical thickness $\delta_{\mathrm{cr,I}}$ (Onset I) corresponding to the critical Rayleigh number, the heat flux encounters a discontinuity as the system switches between conduction and convection. A conductive shell with a slowly declining heat flux will, upon reaching a heat flux of $0.035\ \mathrm{W\,m^{-2}}$ and thickness of 19 km, switch to a convective state at that same heat flux and a thickness of 50 km. Conversely, a convective shell with a slowly increasing heat flux reaches $0.058\ \mathrm{W\,m^{-2}}$ and a 19 km thickness before switching to a conductive state at that same heat flux and a thickness of 10 km. Notice that convective–conductive switches cause larger ice-shell thickness changes than conductive–convective changes; see Mitri and Showman (2005) for a detailed discussion. We emphasize that, if the ice-I shell is close the critical thickness $\delta_{\mathrm{cr,I}}$, a modest perturbation in heat flux can induce *large* and *rapid* changes in the ice-shell thickness. In the convective regime, the rapid fall-off of F with δ at thicknesses of ∼20–50 km corresponds to the 1/5 convective regime, whereas the much more gradual heat flux fall-off at $\delta > 50$ km corresponds to the 1/3 convective regime.

The second panel of Fig. 6 shows the dependence of the heat flux on the thickness of the ice-I shell for an initial ammonia-water concentration of 5% and $d = 0.1$ mm. There are several key points. First, small variations of ammonia concentration change drastically the thermal state of the ice shell. For example, for a heat flux of $0.02\ \mathrm{W\,m^{-2}}$ and $d = 0.1$ mm, the ice shell is in the 1/3 convective regime and has a thickness of ∼145 km for 0% ammonia, but is in the 1/5 convective regime and has a thickness of ∼60 km for 5% ammonia (compare the first and the second panel of Fig. 6). Second, the Onset-I transition in the second panel of Fig. 6 implies that two solutions exist for a range of heat fluxes. In this case, however, the addition of ammonia alters the exact properties of the transition relative to the ammonia-free case. Here, a conductive–convective transition causes a jump in ice-shell thickness from ∼21 to 42 km—as opposed to 19 to 50 km without ammonia. Third, because the addition of ammonia causes a decrease in Rayleigh number at large thicknesses (Fig. 3), a qualitatively new convective–conductive transition occurs—Onset II at a critical thickness of $\delta_{\mathrm{cr,II}} \sim 82$ km for Titan with 5% initial ammonia. Here,

the solution is conductive for $F < 0.006$ W m^{-2} and convective for $F > 0.01$ W m^{-2}, but interestingly, no equilibrium heat flux exists within the range 0.006–0.01 W m^{-2}. This transition therefore differs qualitatively from Onset I because, at Onset II, *no steady-state solutions exist* for a range of heat fluxes from 0.006–0.01 W m^{-2}. For basal heat fluxes within this range, the heat flux transported from below is less than thermal convection can transport but more than thermal conduction can transport. At heat fluxes within this range, the system would be forced to episodically oscillate between convective and conductive regimes on either side of Onset II over a timescale comparable to the thermal diffusion time δ^2/κ, which is ∼200 Myr for a 80-km-thick ice shell. The critical thickness at Onset II could range from ∼40 to ∼150 km depending on the initial ammonia concentration and grain size, which would imply oscillation timescales at Onset II ranging from ∼50 to ∼800 Myr.

We expect the oscillations around Onset II to proceed as follows. Suppose the heat flux available from below lies in the range with no steady-state solution and that we begin on the conductive side of Onset II. The flux transported from below exceeds that conducted through the shell, and this mismatch in heat fluxes causes melting that thins the shell. This thinning drives the system onto the convective side of Onset II. Convective plumes then develop over a thermal diffusion timescale δ^2/κ. As the plumes and convective boundary layers develop, the transported heat flux grows to exceed that available from below, and this mismatch in heat fluxes causes thickening of the shell, which drives the shell onto the conductive side of Onset II. The system will thus repeatedly switch between conductive and convective without reaching an equilibrium.

An inspection of Figs. 4 and 5 shows that, as the ammonia concentration increases, the value of $\delta_{\mathrm{cr,I}}$ increases and $\delta_{\mathrm{cr,II}}$ decreases, implying that the ice-shell thicknesses at Onset I and Onset II converge toward a common value. The thinnest ice shell for which an Onset II transition can occur is ∼40–120 km for both Titan and Enceladus. This situation requires an initial ammonia abundance of ∼10% if $d = 0.1$ mm or ∼0% if $d = 1.0$ mm under Titan conditions, and ∼2.5% if $d = 0.1$ mm under Enceladus conditions. (This corresponds to a dashed curve that barely intersects the dashed–dotted curve in Fig. 4 or Fig. 5.) Larger ammonia abundances imply that convection cannot occur in the ice-I shells under the assumed rheology.

Interestingly, when Onset I and Onset II occur at similar thicknesses, they can interact with each other in a complex manner. Fig. 7 illustrates an example for Enceladus. To visualize this situation, imagine an initially thin, conductive ice shell that slowly thickens in response to a declining basal heat flux. When the flux declines to 0.01 W m^{-2}, the thickening shell reaches Onset I (at a thickness of ∼50 km) and becomes convective. At this point, the convected heat flux far exceeds the available flux transported from below, so the shell attempts to thicken until a new equilibrium is reached. Unlike the case of the second panel of Fig. 6, however, there is no steady-state convective solution for the heat flux of 0.01 W m^{-2}. The shell would therefore thicken until reaching Onset II at a thickness of ∼75 km, and it would be forced to oscillate between conductive and convective states until the basal heat flux decreased below

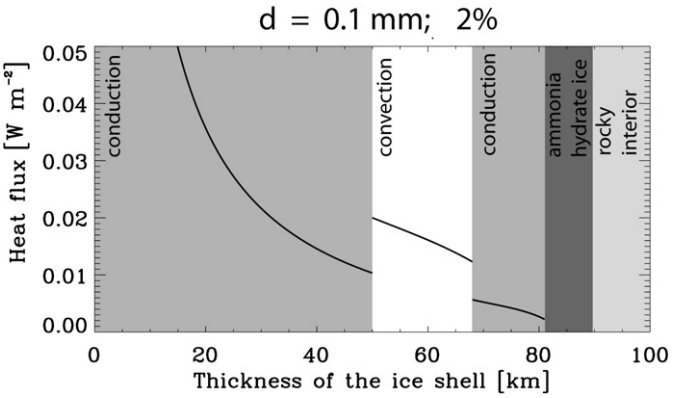

Fig. 7. Heat flux versus thickness of Enceladus' ice-I shell assuming heating from below. The model assumes an ice grain size of 0.1 mm and an initial ammonia-water concentration of 2%. Grey and white areas show where the heat is transported though the ice shell by thermal conduction and convection, respectively. The plot also show where the ice crystallizes as ammonia hydrate ice and the location of the rocky interior.

0.005 W m^{-2}. Thus, in this example, a conductive–convective transition at Onset I (leading to rapid shell thickening) would then induce episodic oscillations between conductive and convective states at Onset II. In this example, the oscillation time would be $\delta^2/\kappa \sim 200$ Myr.

The oscillations between conduction and convection at Onset II could have implications for surface tectonics. A conductive profile has a temperature that decreases steadily from bottom to top of the shell (linearly in the case of constant conductivity and no tidal heating), whereas a convective profile contains a nearly isothermal adiabatic region underlying a stagnant lid. The convective interior temperature is close to the basal temperature and, for $Nu = 1.6$, spans approximately two-thirds of the total ice-I shell thickness. Thus, the mean (height-averaged) interior temperature on the convective side of Onset II would exceed that on the conductive side by up to ∼10–50 K depending on the temperature at the base of the ice shell. Thermal expansion/contraction of the shell could therefore result as the system oscillated from the convective to the conductive side of Onset II. Similarly, conductive–convective oscillations at Onset II are associated with modest oscillations in the thickness of the ice shell (thinner on the conductive side and thicker on the convective side), which in turn cause changes in the volume of the satellite. During the oscillations, the ice-I shell would change in thickness by $\sim\tau\Delta F/L\rho \sim \delta^2\Delta F/\kappa L\rho \sim 10$ km, where $\tau \sim \delta^2/\kappa$ is the oscillation time scale, $L \sim 3\times10^5$ J kg^{-1} is the latent heat, $\rho \sim 1000$ kg m^{-3} is density, and ΔF, which is typically 0.002–0.005 W m^{-2}, is the mismatch in heat flux between that supplied from below and that transported by the ice-I shell at Onset II. The satellite volume change caused by ice-I shell thickness change dominates over thermal expansion. For Enceladus, these arguments imply modest satellite expansion as the system oscillates from convective to conductive and satellite contraction as the system returns from conductive to convective. (The situation is more complex at Titan, because modest ice-I shell thickness changes caused by Onset-II oscillations may induce modest oscillations in the thickness of high-pressure ice phases, which cause a volume change counteracting that of

thickness changes in the ice-I shell.) These effects would lead to surface strains, perhaps reaching $\sim 10^{-3}$, with associated elastic stresses of ~100 bars (which would alternate in sign from one part of the oscillation to another). Repeated oscillations around Onset II could therefore generate surface fractures and deformation, which could be either extensional or compressional depending on whether they formed during the conductive-to-convective or convective-to-conductive phase of the oscillation.

For tectonics, these oscillations around Onset II are interesting because they can cause repeated and extended episodes of surface deformation without requiring unusual behavior of the heat flux supplied to the base of the ice shell. In particular, no oscillations in satellite heat production are needed. A very slowly declining radiogenic heat flux—or even a *constant* heat flux—supplied to the bottom of the shell can cause these repeated convective–conductive oscillations (with associated oscillations in satellite volume and surface heat flux) as long as the heat flux supplied to the bottom of the shell falls within the range necessary for Onset II.

For high initial ammonia-water concentrations, thermal convection cannot occur in the ice. In these cases, all but the thinnest shells are extremely cold at their bases, leading to Rayleigh numbers less than the critical Rayleigh number for all possible shell thicknesses. The third panel of Fig. 6 shows the conductive heat flux dependence on the thickness of the ice shell for Titan assuming an initial ammonia-water concentration of 15% in the liquid sublayer. For an initial ammonia-water concentration of 15%, the liquid layer reaches the eutectic temperature for a thickness of the ice shell of ~70 km and the liquid layer refreezes in ammonia hydrate ice.

Eventually, when the shell is thick enough, the liquid layer reaches the eutectic temperature (177 K) and refreezes completely as ammonia hydrate ice. For an initial ammonia-water concentration of 5% and $d = 0.1$ mm, the liquid layer on Titan reaches the eutectic temperature for a thickness of the ice shell of ~135 km (second panel of Fig. 6). For a pure water liquid layer, the ice reaches the transition from ice-I to ice-III for a thickness of ~160 km (first panel of Fig. 6).

Several factors introduce uncertainties in the locations of the conductive–convective switches in Figs. 4 and 5. As discussed by Barr and McKinnon (2007a, 2007b) and Solomatov and Barr (2006), the critical Rayleigh number given in Eq. (11) is appropriate for an ice shell with arbitrarily small thermal perturbations; an ice shell with large (finite amplitude) thermal perturbations can potentially initiate convection at Rayleigh numbers as low as $\sim 0.6 Ra_{cr}$. Conversely, a convecting ice shell subject to a declining Rayleigh number can potentially sustain so-called *subcritical* convection down to Rayleigh numbers of $\sim 0.6 Ra_{cr}$. In this case, the Nusselt number on the convective side of the transition would be ~1.2–1.3 rather than 1.6. This would have the effect of shifting the conductive–convective boundary upward in Figs. 4 and 5 by a poorly defined increment of order ~10 K. As a result, the amplitudes of the heat flux jumps could potentially be overestimated in Figs. 4 and 7. Additional uncertainties derive from the fact that the critical Rayleigh number depends on the wavelength of thermal perturbations in the ice shell (Turcotte and Schubert, 2002), although this uncertainty is probably unimportant since the Fourier decomposition of any plausible thermal perturbation would have contributions over a broad range of wavelengths. We emphasize, however, that we do not expect these uncertainties to alter the *qualitative* nature of Onsets I and II and their importance for tectonics.

Let us summarize the conditions that could lead to a conductive–convective transition at Onset I or Onset II. For the range of ice-grain sizes we have considered (0.1–1 mm), Titan can encounter Onset I at heat fluxes as large as $\sim 0.05\ \mathrm{W\,m^{-2}}$ or as small as $\sim 0.01\ \mathrm{W\,m^{-2}}$, depending on the ice grain size and initial ammonia concentration; Onset II is encountered at heat fluxes of typically ~ 0.003–$0.01\ \mathrm{W\,m^{-2}}$ (Figs. 4 and 5). Either type of Onset can occur at initial ammonia concentrations up to ~7% when the ice grain size is small (0.1 mm), but this requirement gets stricter as the grain size increases, such that even Titans with ammonia-free oceans cannot undergo conductive–convective switches when the grain size exceeds 1 mm (the shell is always conductive in this case). For Enceladus, a small grain size of 0.1 mm allows Onset I to occur at heat fluxes of ~ 0.008–$0.0015\ \mathrm{W\,m^{-2}}$ and Onset II to occurs at heat fluxes of ~ 0.005–$0.008\ \mathrm{W\,m^{-2}}$, depending on the ammonia abundance; for this grain size, the maximum initial ammonia abundance for either type of Onset is between 2 and 3%.

Is it likely that Titan and Enceladus encountered Onset I and/or Onset II during their histories? For Titan, the expected radiogenic heating (assuming chondritic radionuclide abundances in the rocky portion) ranged from $\sim 0.04\ \mathrm{W\,m^{-2}}$ early in Solar System history to $\sim 0.003\ \mathrm{W\,m^{-2}}$ today according to the abundances in Kirk and Stevenson (1987); tidal heating could have increased these fluxes by a modest amount. Tobie et al. (2005a, 2005b) have estimated a present tidal + radiogenic heat flux of $0.007\ \mathrm{W\,m^{-2}}$. According to these numbers, it is likely that Titan has encountered Onset I, but Onset II is less likely because Titan's heat flux may always have been too high. For Enceladus, the radiogenic heating flux is over an order of magnitude lower than on Titan, but tidal heating probably makes up the difference, at least episodically. The episodic nature of the resurfacing on Enceladus (Kargel and Pozio, 1996) suggests that Enceladus' heat flux may have varied in time, perhaps by a large factor. If Enceladus' tidal heat flux has varied episodically, as is plausible, then the satellite could have readily passed through both Onset I and Onset II during its history.

3.3. Radial expansion and contraction

During a conductive–convective transition an ice-I shell undergoes a drastic change of its thermal state. Mitri and Showman (2005) have shown that the conductive–convective transition produces a radial expansion of Europa. McKinnon (2006) has discussed the tectonic effects and the thermal reorganization of the Callisto ice-I shell due to the thermal state switch. In contrast to Europa, high-pressure ice polymorphs (with a mean density of $\sim 1300\ \mathrm{kg\,m^{-3}}$) could exist on Titan between the ocean and the rocky interior. During the cooling of the planet, the radial expansion of the ice-I layer is, in general, counterbalanced by the radial contraction of the ice high pressure layer. Therefore, a global contraction of Titan could occur during its

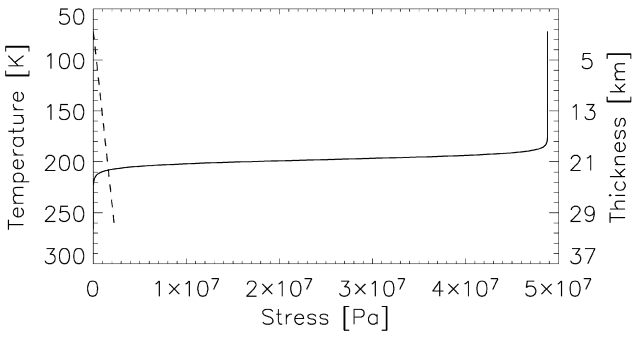

Fig. 8. Stress and fracture depth during the radial expansion of Enceladus for an ice grain size of 0.1 mm and an initial ammonia-water concentration of 0.5%. The left-hand axis shows the temperature in the ice shell, and the right-hand axis shows the depth within the ice shell. The dashed line shows the lithostatic stress given by $\sigma_{\rm lit} = \rho g h$, where ρ is the ice density, g is the Enceladus gravity (0.114 m s^{-2}), and h is the depth within the ice shell. The cracks propagate from the surface downward when the expansion stress reaches the lithostatic stress. For the low gravity of Enceladus and the high fractional volume change during a conductive–convective transition, the cracks propagate to a depth of ∼21 km.

cooling. The radial contraction of Titan could build compressive surface structures.

Like Europa, Enceladus lacks a high-pressure ice polymorph layer. Because Enceladus could have recently undergone a period of tidal heating (Wisdom, 2004), it is particularly interesting to investigate the influence of a change of heat production on the ice layer. Supposing that the Enceladus ice shell has undergone a conductive–convective transition, we determine the depth and dimension of extensional fractures during a thermal state switch.

We compute the stress during the radial expansion as function of the ice shell temperature using the flow law of a Maxwellian viscoelastic body given by

$$\dot{\varepsilon}(t) = \frac{\dot{\sigma}}{\mu} + \frac{\sigma}{\eta} + A\frac{\sigma^n}{d^p}\exp\left(\frac{Q}{RT}\right), \tag{13}$$

where $\dot{\varepsilon}(t)$ is the strain rate, $\dot{\sigma}(t)$ is the derivation in time t of the stress σ, μ is the rigidity of the ice (4×10^9 Pa), η is the temperature dependent viscosity, A, n, p are constants, d is the grain size, Q is the activation energy, R is the gas constant, and T is the temperature.

Under Enceladus' surface conditions, dislocation and diffusion creep are predominant. Therefore, the third term of Eq. (8) represents the dislocation creep with $n = 4$, $Q = 60$ kJ mol^{-1} and $p = 0$ (Goldsby and Kohlstedt, 2001). We write the strain rate $\dot{\varepsilon}$ as a Gaussian (Showman et al., 1997; Mitri and Showman, 2005)

$$\dot{\varepsilon} = \frac{\Delta V}{3V}\frac{1}{\tau\sqrt{\pi}}\exp\left[-\frac{(t-3\tau)^2}{\tau^2}\right], \tag{14}$$

where t is the time, τ is the characteristic time scale, and $\Delta V/V$ is the fractional volume expansion.

For $d = 0.1$ mm and an initial ammonia-water concentration of 0.5%, a conductive–convective transition causes a refreezing of ∼35 km (Fig. 5), corresponding to a radial expansion of ∼3 km and a linear extensional strain of 0.012 at the surface. The expected increase in surface area is 2×10^4 km^2; extensional fracture, graben formation, and perhaps necking instabilities could occur, helping to explain Enceladus' rifted terrain (Kargel and Pozio, 1996). The fractional volume expansion of Enceladus is $\Delta V/V \sim 0.0366$, and the conductive–convective transition occurs for a heat flux from the interior of the satellite of $F \sim 0.013$ W m^{-2}. We assumed a surface temperature of 70 K for this calculation. The ice shell refreezes in a timescale $\tau \sim 2 \times 10^7$ years, and the maximum surface stress is almost 500 bars (Fig. 8). Fig. 8 shows the stress and fracture depth during the radial expansion of Enceladus. The left-hand vertical axis shows the temperature in the ice shell, and the right-hand vertical axis shows the depth below the surface. The dashed line shows the lithostatic stress given by $\sigma_{\rm lit} = \rho g \delta$, where ρ is the ice density, g is the Enceladus gravity (0.114 m s^{-2}), and δ is the ice shell thickness. The cracks propagate to depths at least as great as the depth where the solid and dashed curves cross. For the low gravity of Enceladus and the high fractional volume change during a conductive–convective transition, the cracks propagate to a depth of ∼21 km (Fig. 8). The penetration depth of the cracks during a conductive–convective transition could help produce conduits through which warm ice or ammonia-water liquid might reach the surface, helping to explain the extensive resurfacing (Kargel and Pozio, 1996).

4. Conclusions

We have demonstrated that thermal convection in stagnant lid regime can occur in the ice shells of Titan and Enceladus under a range of conditions. Because of the dependence of Rayleigh number on δ^3/η_b where δ is the thickness of the ice shell and η_b is the viscosity at the base of the ice shell, and because ammonia in the liquid layer acts as an antifreeze, the Rayleigh number equals its critical value for two thicknesses: for a thin ice shell with a warm, low-viscosity base (Onset I) and for a thick ice shell with a cold, high-viscosity base (Onset II). In previous work we demonstrated that for a fluid with temperature-dependent viscosity, at the critical Rayleigh number the Nusselt number undergoes a discontinuous jump from ∼1 to 1.6–1.7 (Mitri and Showman, 2005). With increasing ice-shell thickness, two finite-amplitude discontinuities of the Nusselt number can therefore occur: the first at $\delta_{\rm cr,I}$ and the second at $\delta_{\rm cr,II}$.

Interestingly, near Onset I, *two* ice-shell equilibria exist for a range of heat fluxes (one a thin, conductive state and the other a thicker, convective state) (Mitri and Showman, 2005), but near Onset II, *zero* equilibria exist for a range of heat fluxes. A system with a time-averaged heat flux within that range would be forced to episodically oscillate between conductive and convective states (with ∼70% variations in the surface heat flux) without ever reaching a steady state.

Depending on the interior ammonia abundance and the detailed history of radiogenic and tidal heating, the system could pass through Onset I, Onset II, or both throughout Solar System history, possibly multiple times if the internal heating rates is episodic (as it may be on Enceladus; Wisdom, 2004). These events could have important implications for the internal evolution and surface tectonics.

We have demonstrated that the Onset I of Enceladus ice shell floating on an ocean produces tectonic stress of ∼500 bars and fractures of few tens of km depth. Conductive–convective oscillations around Onset II could occur on timescales of ∼50–800 Myr and cause stresses up to ∼100 bars. The penetration depth of the cracks during a conductive–convective transition could help allow resurfacing of Enceladus or Titan with warm ice or water from a liquid subsurface layer. During the cooling of Titan, the radial expansion of the ice-I layer is, in general, counterbalanced by the radial contraction of the ice high pressure layer.

Acknowledgments

This work was support in part by NASA PG&G Grant NNG04GI46G to A.P.S. Part of the research work was carried out while G.M. was at the Lunar and Planetary Laboratory, University of Arizona. G.M. was supported in part by an appointment to the NASA Postdoctoral Program at the Jet Propulsion Laboratory.

References

Barr, A.C., McKinnon, W.B., 2007a. Convection in ice I shells and mantles with self-consistent grain size. J. Geophys. Res. 112. 2012.

Barr, A.C., McKinnon, W.B., 2007b. Convection in Enceladus' ice shell: Conditions for initiation. Geophys. Res. Lett. 34. 9202.

Barr, A.C., Pappalardo, R.T., 2005. Onset of convection in the icy Galilean satellites: influence of rheology. J. Geophys. Res. 110, doi:10.1029/2004JE002371. E12005.

Collins, G., Goodman, J.C., 2007. Enceladus' south polar sea. Icarus 189, 72–82.

Croft, S.K., Lunine, J.I., Kargel, J., 1988. Equation of state of ammonia-water liquid—Derivation and planetological applications. Icarus 73, 279–293.

Dermott, S.F., Thomas, P.C., 1994. The determination of the mass and mean density of Enceladus from its observed shape. Icarus 109, 241–257.

Deschamps, F., Sotin, C., 2000. Inversion of two-dimensional numerical convection experiments for a fluid with a strongly temperature-dependent viscosity. Geophys. J. Int. 143, 204–218.

Dumoulin, C., Doin, M.P., Fleitout, L., 1999. Heat transport in stagnant lid convection with temperature- and pressure-dependent Newtonian or non-Newtonian rheology. J. Geophys. Res. 104, 12759–12777.

Durham, W.B., Kirby, S.H., Stern, L.A., 1997. Creep of water ices at planetary conditions: A compilation. J. Geophys. Res. 102, 16293–16302.

Elachi, C., and 34 colleagues, 2006. Titan Radar Mapper observations from Cassini's T3 fly-by. Nature 441, 709–713.

Goldsby, D.L., Kohlstedt, D.L., 2001. Superplastic deformation of ice: Experimental observations. J. Geophys. Res. 106, 11017–11030.

Grasset, O., Sotin, C., 1996. The cooling rate of a liquid shell in Titan's interior. Icarus 123, 101–112.

Grasset, O., Sotin, C., Deschamps, F., 2000. On the internal structure and dynamics of Titan. Planet. Space Sci. 48, 617–636.

Hussmann, H., Sohl, F., Spohn, T., 2006. Subsurface oceans and deep interiors of medium-sized outer planet satellites and large trans-neptunian objects. Icarus 185, 258–273.

Kargel, J.S., 1992. Ammonia-water volcanism on icy satellites—Phase relations at 1 atmosphere. Icarus 100, 556–574.

Kargel, J.S., Pozio, S., 1996. The volcanic and tectonic history of Enceladus. Icarus 119, 385–404.

Kirk, R.L., Stevenson, D.J., 1987. Thermal evolution of a differentiated Ganymede and implications for surface features. Icarus 69, 91–134.

Leliwa-Kopystynski, J., Maruyama, M., Nakajima, T., 2002. The water–ammonia phase diagram up to 300 MPa: Application to icy satellites. Icarus 159, 518–528.

Lopes, R.M.C., and 43 colleagues, 2007. Cryovolcanic features on Titan's surface as revealed by the Cassini Titan Radar Mapper. Icarus 186, 395–412.

Lunine, J.I., Stevenson, D.J., Yung, Y.L., 1983. Ethane ocean on Titan. Science 222, 1229–1230.

McKinnon, W.B., 1999. Convective instability in Europa's floating ice shell. Geophys. Res. Lett. 26, 951–954.

McKinnon, W.B., 2006. On convection in ice I shells of outer Solar System bodies, with detailed application to Callisto. Icarus 183, 435–450.

Mitri, G., Showman, A.P., 2005. Convective conductive transitions and sensitivity of a convecting ice shell to perturbations in heat flux and tidal-heating rate: Implications for Europa. Icarus 177, 447–460.

Moore, W.B., 2006. Thermal equilibrium in Europa's ice shell. Icarus 180, 141–146.

Moresi, L.N., Solomatov, V.S., 1995. Numerical investigation of 2D convection with extremely large viscosity variations. Phys. Fluids 7, 2154–2162.

Mousis, O., Gautier, D., Bockelée-Morvan, D., 2002. An evolutionary turbulent model of Saturn's subnebula: Implications for the origin of the atmosphere of Titan. Icarus 156, 162–175.

Nimmo, F., Pappalardo, R.T., 2006. Diapir-induced reorientation of Saturn's moon Enceladus. Nature 441, 614–616.

Porco, C.C., and 24 colleagues, 2006. Cassini observes the active south pole of Enceladus. Science 311, 1393–1401.

Radebaugh, J., Lorenz, R., Kirk, R., Lunine, J., and Cassini Radar Team, 2006. Mountains on Titan observed by Cassini Radar. Lunar Planet. Sci. 37. Abstract 1007.

Schubert, G., Anderson, J.D., Travis, B.J., Palguta, J., 2007. Enceladus: Present internal structure and differentiation by early and long-term radiogenic heating. Icarus 188, 345–355.

Showman, A.P., Han, L., 2004. Numerical simulations of convection in Europa's ice shell: Implications for surface features. J. Geophys. Res. 109 (E1), doi:10.1029/2003JE002103. E01010.

Showman, A.P., Stevenson, D.J., Malhotra, R., 1997. Coupled orbital and thermal evolution of Ganymede. Icarus 129, 367–383.

Solomatov, V.S., 1995. Scaling of temperature- and stress-dependent viscosity convection. Phys. Fluids 7, 266–274.

Solomatov, V.S., Barr, A.C., 2006. Onset of convection in fluids with strongly temperature-dependent, power-law viscosity. Phys. Earth Planet. Int. 155, 140–145.

Solomatov, V.S., Moresi, L.N., 1996. Stagnant lid convection on Venus. J. Geophys. Res. 101, 4737–4754.

Solomatov, V.S., Moresi, L.N., 1997. Erratum: "Stagnant lid convection on Venus". J. Geophys. Res. 102, 28729.

Solomatov, V.S., Moresi, L.N., 2000. Scaling of time-dependent stagnant lid convection: Application to small-scale convection on Earth and other terrestrial planets. J. Geophys. Res. 105, 21795–21818.

Sotin, C., Grasset, O., Beauchesne, S., 1997. Thermodynamic properties of high pressure ices: Implications for the dynamics and internal structure of large icy satellites. In: Schmitt, B., et al. (Eds.), Solar System Ices, pp. 79–96.

Spencer, J.R., Pearl, J.C., Segura, M., Flasar, F.M., Mamoutkine, A., Romani, P., Buratti, B.J., Hendrix, A.R., Spilker, L.J., Lopes, R.M.C., 2006. Cassini encounters Enceladus: Background and the discovery of a south polar hot spot. Science 311, 1401–1405.

Squyres, S.W., Reynolds, R.T., Cassen, P.M., 1983. The evolution of Enceladus. Icarus 53, 319–331.

Stevenson, D.J., 1982. Volcanism and igneous processes in small icy satellites. Nature 298, 142–144.

Tobie, G., Mocquet, A., Sotin, C., 2005a. Tidal dissipation within large icy satellites: Applications to Europa and Titan. Icarus 177, 534–549.

Tobie, G., Grasset, O., Lunine, J.I., Mocquet, A., Sotin, C., 2005b. Titan's internal structure inferred from a coupled thermal-orbital model. Icarus 175, 496–502.

Tobie, G., Lunine, J.I., Sotin, C., 2006. Episodic outgassing as the origin of atmospheric methane on Titan. Nature 440, 61–64.

Turcotte, D.L., Schubert, G., 2002. Geodynamics. Cambridge Univ. Press, Cambridge, UK.

Waite, J.H., and 13 colleagues, 2006. Cassini Ion and Neutral Mass Spectrometer: Enceladus plume composition and structure. Science 311, 1419–1422.

Wisdom, J., 2004. Spin–orbit secondary resonance dynamics of Enceladus. Astron. J. 128, 484–491.